

The European Low Frequency Survey

Observing the radio sky to understand the beginning of the Universe

A. Mennella^{1,2,*}, K. Arnold³, S. Azzoni⁴, C. Baccigalupi⁵, A. Banday⁶, R.B. Barreiro⁷, D. Barron⁸, M. Bersanelli^{1,2}, S. Casey³, L. Colombo^{1,2}, E. de la Hoz^{9,10}, C. Franceschet^{1,2}, M.E. Jones¹¹, R.T. Genova-Santos^{12,13}, R.J. Hoyland^{12,13}, A.T. Lee¹⁰, E. Martinez-Gonzalez⁷, F. Montonati¹, J.A. Rubiño-Martin^{12,13}, A. Taylor¹¹, and P. Vielva⁷

¹Università degli studi di Milano, Milano, Italy

²Istituto Nazionale di Fisica Nucleare (INFN) sezione di Milano, Milano, Italy

³University of California San Diego, La Jolla, CA 92093-0021, USA

⁴Princeton University, Princeton, NJ 08544, USA

⁵Scuola Internazionale Superiore di Studi Avanzati (SISSA), Trieste, Italy

⁶Institut de Recherche end Astrophysique et Planétologie (IRAP), Toulouse, France

⁷Instituto de Física de Cantabria (IFCA), Santander, Cantabria, Spain

⁸The University of New Mexico, Albuquerque, NM 87131, USA

⁹Centre Pierre Binétruy (CNRS-UCB), IRL2007, CPB-IN2P3, Berkeley, CA 94720, USA

¹⁰Berkeley University of California, Berkeley, CA 94720-4206, USA

¹¹University of Oxford, Oxford OX1 2JD, United Kingdom

¹²Instituto de Astrofísica de Canarias, La Laguna, Tenerife, Spain

¹³Departamento de Astrofísica, Universidad de La Laguna, Tenerife, Spain

Abstract. In this paper we present the European Low Frequency Survey (ELFS), a project that will enable foregrounds-free measurements of primordial B -mode polarization to a level 10^{-3} by measuring the Galactic and extra-Galactic emissions in the 5–120 GHz frequency window. Indeed, the main difficulty in measuring the B -mode polarization comes not just from its sheer faintness, but from the fact that many other objects in the Universe also emit polarized microwaves, which mask the faint CMB signal. The first stage of this project will be carried out in synergy with the Simons Array (SA) collaboration, installing a 5.5–11 GHz coherent receiver at the focus of one of the three 3.5 m SA telescopes in Atacama, Chile (“ELFS on SA”). The receiver will be equipped with a fully digital back-end based on the latest Xilinx RF System-on-Chip devices that will provide frequency resolution of 1 MHz across the whole observing band, allowing us to clean the scientific signal from unwanted radio frequency interference, particularly from low-Earth orbit satellite mega-constellations. This paper reviews the scientific motivation for ELFS and its instrumental characteristics, and provides an update on the development of ELFS on SA.

1 Introduction

The high-fidelity subtraction of galactic foreground emission may be the largest single challenge to detecting the signature of primordial gravitational waves that could be generated

*e-mail: aniello.mennella@fisica.unimi.it

by inflation shortly after the Big Bang. The target sensitivity of $r \sim 10^{-3}$ in the next generation CMB experiments, such as Simons Observatory (SO) implies that foregrounds are at least an order of magnitude higher in brightness.

There has been a great focus on the Galactic dust foreground, especially after the claimed BICEP2 B -mode detection turned out to be emission from dust. The level of complexity of the dust emission is not yet fully known, and it is recognized by the CMB community that dust has to be very well understood to rule out its role in a future claim of B -modes detection. Synchrotron radiation is less well characterized and potentially more complex than dust. As measurements become deeper, synchrotron could become a bigger obstacle than dust if its spectrum turns out to be highly complex.

Our current knowledge of the synchrotron radiation has increased significantly after ground-based experiments operating in the 2–20 GHz range: S-PASS (2.3 GHz) [1] in the Southern Hemisphere, C-BASS (5 GHz) [2] and QUIJOTE-MFI (10–20 GHz) [3] in the Northern Hemisphere. These data highlight that the synchrotron emission is more complex than has been assumed in CMB forecast codes. Data from low-frequency instruments will be key in constraining and removing the synchrotron emission to extract the CMB signal.

The European Low Frequency Survey (ELFS) is a long-term plan to deploy dedicated telescopes to produce a full-sky survey in the 5–100 GHz range with an unprecedented level of angular resolution (~ 20 arcmin at 10 GHz), sub-GHz spectral resolution and sensitivity that will allow B -mode extraction from data produced by LiteBIRD, Simons Observatory and CMB-Stage 4 measurements. A first step (that we call ELFS on SA) is the deployment of a 6–12 GHz receiver (hereafter P6/12) in the Gregorian focus of one of the Simons Array telescopes [4], followed by the installation of the QUIJOTE-MFI2 [5] to cover the 10–20 GHz range.

In this paper we briefly review the instrumental characteristic of the P6/12 receiver and show the impact of ELFS on SA measurements when combined with those expected from the Simons Observatory.

2 ELFS on Simons Array: the P6/12 instrument

In Table 1 we report the main instrumental performance in terms of frequency bands, angular resolution and noise of the P6/12 receiver. A schematic of the main components is reported in Fig. 1.

Table 1. Top-level performance parameters of the P6/12 receiver. N^P indicates the noise level in polarization.

ν [GHz]	θ_{FWHM} [arcmin]	N^P [$\mu\text{K}\cdot\text{arcmin}$]	ℓ_{knee}	α_{knee}
6.3	46.6	539	15	-2.4
7.0	42.2	512	15	-2.4
7.7	38.1	487	15	-2.4
8.6	34.4	465	15	-2.4
9.5	31.1	443	15	-2.4
10.5	28.1	423	15	-2.4

The top-left panel of Fig. 1 shows the feedhorn mechanical design with the main dimensions. Following the ideas presented in [6] we have designed it with a hyperbolic profile and a ring-loaded slot mode converter. The corrugation teeth are 4.5 mm in the body of the horn and 5 mm in the mode converter part, with constant tooth/groove ratio of 0.889. This con-

figuration allowed us to obtain excellent broadband performance in terms of return loss and cross-polarization performance, as shown in the top-center and top-right plots of Fig. 1.

The orthomode transducer (OMT) is based on a design being used for the Square Kilometre Array Band 5a and 5b feeds. This is a quad-ridge design in which the ridges for one polarization are held at a constant spacing while they pass by the coaxial probe and backshort of the other polarization. This design reduces coupling between the polarizations and allows for a bandwidth of more than 2:1 with minimal excitation of higher order modes. The OMT is manufactured in four quadrants which are assembled with precision dowels to set the critical spacings between the ridges, which then requires no further tuning.

The OMT will be incorporated into a cryostat adapted from the C-BASS North receiver [7]. This is based on a Sumitomo SRDK-408D2 two-stage Gifford-McMahon cold head that reaches a base temperature of 4 K. The cryostat cold plate can be interfaced up to four low-noise amplifiers plus the associated planar hybrid modules to allow for the continuous comparison radiometer architecture used in C-BASS. It will be modified to accommodate the new 2:1 bandwidth OMT in place of the 30% bandwidth OMT used in C-BASS.

As ELFS is focussed on polarization measurements for which the continuous comparison architecture is not necessary, we will use just two RF channels, using a planar 90-degree hybrid to convert the linear OMT outputs to circular polarization, and two Low Noise Factory LNF_LNC4_16C amplifiers to provide the primary gain (see bottom panel of Fig. 1). Coaxial 30 dB couplers in the RF lines before the LNAs will allow us to inject a noise signal for calibration in to both circular polarizations.

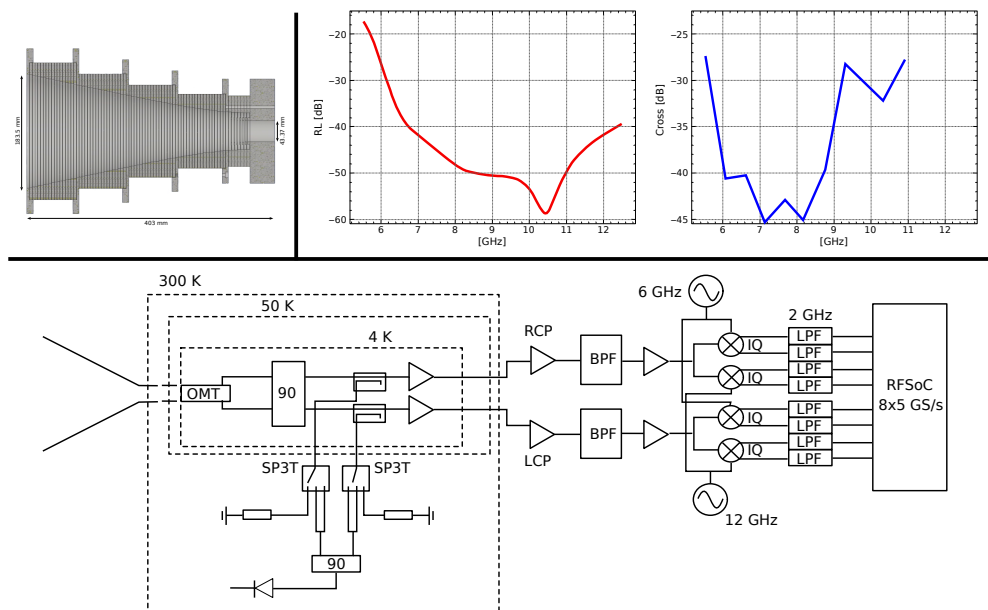


Figure 1. *Top panel:* electromagnetic model of the corrugated feedhorn (left), simulated return loss (center) and cross-polarization (right). *Bottom panel:* receiver schematic.

The backend will follow the design philosophy of the QUIJOTE-MF12 instrument [5], using an FPGA based digital backend. The MF12 FPGA (Xilinx ZCU208 Ultrascale) has the capability to simultaneously acquire eight RF channels at a sampling frequency of 5.0 GSps,

a 2.5 GHz band and 1 MHz spectral resolution. The full bandwidth will be divided into spectral sub-bands with maximum bandwidth of 2.5 GHz, which are down-converted to base band [0, 2.5] GHz through separate Local Oscillators (LOs). In the P6/12 design this will be achieved by using the complex output of mixers to achieve two bands from any LO.

The backend design implements a hard programmed polyphase filterbank and a fast Fourier transform to retrieve the spectral information from the digitised samples of the fast onboard ADCs in the time domain. The power spectral density is then integrated in time and averaged. A temporary storage space is used to store 24 h of raw data which is used to find an optimum blocking filter for any undesired interference. The final stored scientific signal is a spectral average with an averaging factor that depends on the scientific needs and the available storage space.

3 Expected impact on science

To assess the impact of adding low frequency channels in foreground and CMB data analysis, we considered the Simons Observatory¹ (SO) experiment combined with ELFS-SA channels (the P6/12 and the QUIJOTE-MFI2 instruments), as shown in panel (a) of Fig. 2, which shows frequencies and sensitivities.

Our simulations include a sky signal with the CMB, synchrotron emission with or without curvature (i.e., frequency-dependent spectral index), and thermal dust emission. We used d10 and s5 PySM models [8] to simulate the thermal dust and the synchrotron emission without curvature. To simulate the synchrotron with a curved spectrum we generated a custom model with the same spectral index as s5 and a curvature template whose values are allowed by current observations in the Southern Hemisphere. This template is created by mean shifting to achieve a final mean of 0.04 and rescaling the spatial variations by a factor of ~ 30 the PySM s7 template. We emphasize that neither the sky model nor the cleaning procedure was validated through the SO pipeline presented in Wolz et al. [9].

In the right panel of Fig. 2, we display the fitted synchrotron spectral index for various instrument configurations. It shows that, for the synchrotron model considered, a good characterization is reached by combining ELFS with SO. The first row shows the case where synchrotron follows a power-law and is fitted with a power-law. The second row represents the scenario where synchrotron has a curved spectral index but is fitted with a power-law. Lastly, the third row demonstrates the case where curved synchrotron is fitted with the correct model. The bias observed in the second row of fits with ELFS confirms that including low-frequency channels allows us to detect synchrotron curvature.

Figure 3 shows the reduced χ^2 from the synchrotron fits obtained using SO alone (left) or ELFS-SA plus SO (right). The comparison of the top and bottom rows shows how the existence of an extra parameter in synchrotron complexity may be effectively constrained by the combination of ELFS and SO data. When we include the information from ELFS on SA, we observe differences between the two simulated skies, obtaining the best fit when we fit the synchrotron using the correct model.

Figure 4 shows the recovered tensor-to-scalar-ratio when the sky is modeled using the d10sC foreground models, in two cases: without delensing, and assuming a 50% delensing. The r value shown corresponds to the value obtained with the best-fit model from the χ^2_{red} maps, i.e., the power-law model in the case of SO alone, and power-law with curvature when we add the instruments from ELFS on SA. Results indicate how the bias on r can be mitigated when ELFS and SO data are combined. The value of r remains somewhat biased due to the challenge of accurately determining the true combination of β_s and c_s values, which are strongly degenerate. We are currently exploring approaches to mitigate this bias, including

¹We include the additional SATs from SO:UK and SO:JP as well as an extended observation time (until 2035).

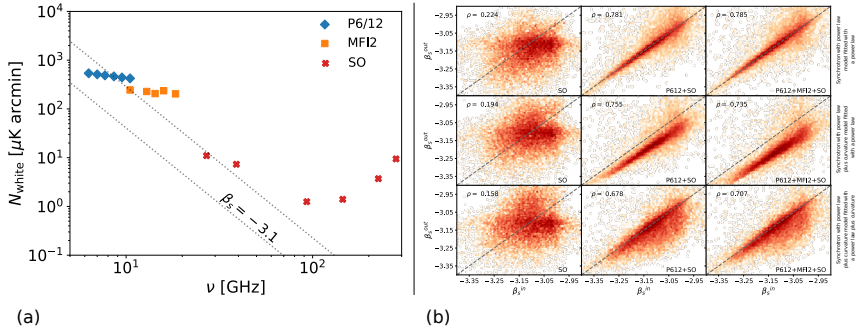


Figure 2. (a) Sensitivity of the tested instrument configurations as a function of frequency. The dotted line shows the extrapolated sensitivity following a power law with a -3.1 exponent. (b) Comparison of recovered β_s values to input β_s values for all observable pixels from Atacama. From left to right: SO, P612+SO, and P612+MFI2+SO results. The dashed diagonal represents $\beta_s^{\text{out}} = \beta_s^{\text{in}}$. The correlation coefficients (ρ) are displayed in the upper left of each plot.

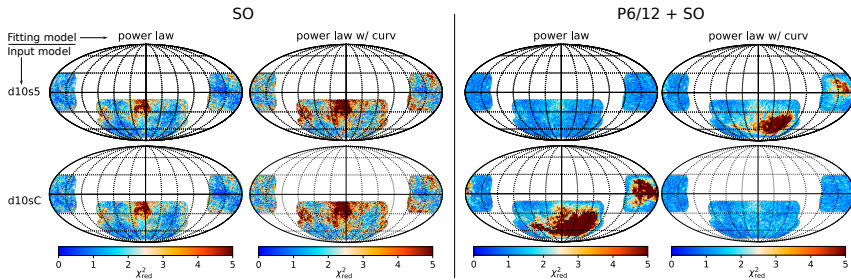


Figure 3. Reduced χ^2 maps generated using SO data alone and ELFS+SO data. The top (bottom) row corresponds to simulations using the d10s5 (d10sC) model, where synchrotron is represented as a power law (power law with curvature). The odd columns display the maps obtained with a power law model fitting the synchrotron emission, while the even columns present the χ_{red}^2 values when the synchrotron is modeled with a power law with curvature.

the incorporation of prior information related to the effective exponent in the power-law with curvature model to break the parameter degeneracy and enhancing the sensitivity of the P6/12.

These results highlight the importance of low-frequency data in discerning complex synchrotron behavior, extending beyond a basic power-law model. Furthermore, in the latter case, these data will help mitigate the residuals coming from the synchrotron emission.

4 Conclusions

In this paper we have presented ELFS, a plan to deploy dedicated telescopes to produce a full-sky survey in the 5–100 GHz range, and its first incarnation, ELFS on SA, which foresees the deployment of a 6–12 GHz receiver in the Gregorian focus of one of the Simons Array telescopes, followed by the installation of the QUIJOTE-MFI2 to cover the 10–20 GHz range. We have analyzed the potential of ELFS on SA in discerning complex synchrotron behavior, when combined with measurements from next generation experiments, like the Simons Observatory. Our results show that the complexity of synchrotron cannot be underestimated and

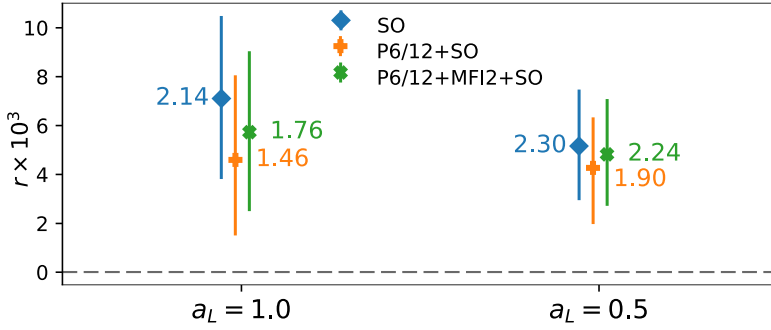


Figure 4. The tensor-to-scalar ratio recovery, simulated with d10sC foregrounds, varies with the amount of included lensing in the CMB simulations. Blue diamonds, orange plus signs, and green crosses represent values obtained using the best-fit model for SO, P6/12+SO, and P6/12+MFI2+SO data, respectively. This involves using a power-law model for SO alone and a power-law with curvature when including low-frequency data.

the availability of high precision, low frequency observations will be of key importance in presence of a potential tensor-to-scalar ratio detection.

Acknowledgements

This is not an official SO Collaboration paper.

References

- [1] N. Krachmalnicoff, E. Carretti, C. Baccigalupi, G. Bernardi, S. Brown, B.M. Gaensler, M. Haverkorn, M. Kesteven, F. Perrotta, S. Poppi et al., *ApJ* **618**, A166 (2018), 1802.01145
- [2] M.E. Jones, A.C. Taylor, M. Aich, C.J. Copley, H.C. Chiang, R.J. Davis, C. Dickinson, R.D.P. Grumitt, Y. Hafez, H.M. Heilgendorff et al., *MNRAS* **480**, 3224 (2018), 1805.04490
- [3] J.A. Rubiño-Martín, F. Guidi, R.T. Génova-Santos, S.E. Harper, D. Herranz, R.J. Hoyland, A.N. Lasenby, F. Poidevin, R. Rebolo, B. Ruiz-Granados et al., *MNRAS* **519**, 3383 (2023), 2301.05113
- [4] D. Barron, et al., in *American Astronomical Society Meeting Abstracts #231* (2018), Vol. 231 of *American Astronomical Society Meeting Abstracts*, p. 356.02
- [5] R.J. Hoyland, J.A. Rubiño-Martín, M. Aguiar-Gonzalez, P. Alonso-Arias, E. Artal, M. Ashdown, R.B. Barreiro, F.J. Casas, C. Colodro-Conde, E. de la Hoz et al., in *Millimeter, Submillimeter, and Far-Infrared Detectors and Instrumentation for Astronomy XI*, edited by J. Zmuidzinas, J.R. Gao (2022), Vol. 12190 of *Society of Photo-Optical Instrumentation Engineers (SPIE) Conference Series*, p. 1219033
- [6] C. Granet, G. James, *IEEE Antennas and Propagation Magazine* **47**, 76 (2005)
- [7] O.G. King, M.E. Jones, E.J. Blackhurst, C. Copley, R.J. Davis, C. Dickinson, C.M. Holler, M.O. Irfan, J.J. John, J.P. Leahy et al., *MNRAS* **438**, 2426 (2014), 1310.7129
- [8] B. Thorne, J. Dunkley, D. Alonso, S. Naess, *MNRAS* **469**, 2821 (2017), 1608.02841
- [9] K. Wolz, S. Azzoni, C. Hervias-Caimapo, J. Errard, N. Krachmalnicoff, D. Alonso, C. Baccigalupi, A. Baleato Lizancos, M.L. Brown, E. Calabrese et al., arXiv e-prints arXiv:2302.04276 (2023), 2302.04276